Eur. Phys. J. D **4**, 159–168 (1998)

THE EUROPEAN PHYSICAL JOURNAL D

Reaction and inelastic processes in the collision O_2 ($v \gg 0$) + O_2 ($v = 0$)

J. Campos-Martínez[1,a], E. Carmona-Novillo[1], J. Echave[2], M.I. Hernández[1], R. Hernández-Lamoneda[3], and J. Palma[2]

[1] Instituto de Matemáticas y Física Fundamental (C.S.I.C.), Serrano 123, 28006-Madrid, Spain
[2] Centro de Estudios e Investigaciones, Universidad Nacional de Quilmes, R. Saenz Peña 180, 1876 Bernal, Argentina
[3] Facultad de Ciencias,Universidad Autónoma del Estado de Morelos, 62210 Cuernavaca, Morelos, Mexico

Received: 3 February 1998 / Revised: 27 March 1998 / Accepted: 15 May 1998

Abstract. A reduced dimensionality model is used to study the reaction $O_2(X^3\Sigma_g^-, v \gg 0)+O_2(^3\Sigma_g^-, v' = 0) \rightarrow O_3(X^1A_1)+ O(^3P)$ by means of time-dependent and time-independent quantum-mechanical methods. State-selected probabilities and rate constants are obtained for the reactive process as well as for the inelastic collision in which the vibrationally excited oxygen loses one or more quanta. It is found that the experimentally observed jump in depletion rates above a critical value of v could be partially explained by the vibrational relaxation rather than reaction. Reaction only becomes important for relatively high translational energies and therefore the calculated rates are too small at the temperatures of interest. It is concluded, however, that the reaction saddle point region in the potential energy surface plays a crucial role in the enhancement of vibrational relaxation.

PACS. 34.10.+x General theories and models of atomic and molecular collisions and interactions (including statistical theories, transition state, stochastic and trajectory models, etc.) – 34.50.Ez Rotational and vibrational energy transfer – 82.40.We Atmospheric chemistry

1 Introduction

The study of atmospheric processes involving vibrationally excited oxygen molecules has attracted an increasing interest in the last few years. Several suggestions [1,2] have been made on the role of $O_2^\ddagger$ to help solving the so-called "ozone deficit problem" [3], which in simple terms reflects the fact that a higher stratospheric ozone concentration is experimentally recorded than predicted by model simulations. Although recent analyses and observations [4,5] seem to overcome this problem, this is still a controversial matter that has produced a renewed debate in ozone chemistry. Even if the ozone deficit problem were solved, $O_2^\ddagger$ molecules are of great importance in their own for atmospheric modeling purposes.

Some years ago, Slanger *et al.* [1] proposed a new ozone production mechanism in which vibrationally hot $O_2(X^3\Sigma_g^-)$ molecules could be photolyzed by sunlight. The nascent oxygen atoms could react with ground state O_2 yielding a net production of ozone. Vibrationally excited oxygen appears in the photolysis of ozone below 248 nm with typical bimodal distributions [6–8] peaked around $v = 14$ and $v = 27$. However, a crucial point in the Slanger autocatalitic mechanism is the requirement that collisional relaxation must be slow compared with solar photodissociation. When measurements [9,10] showed that collisional relaxation was very fast, this mechanism had to be abandoned and new propositions were required.

In a series of works Wodtke and co-workers [10,11] carried out detailed stimulated emission pumping (SEP) experiments designed to measure the depletion rate of $O_2(X^3\Sigma_g^-, v)$ in collision with O_2 molecules in the vibrational ground state. In those experiments, different vibrationally excited states were populated by a sequence of pump-dump lasers and their decay was monitored with an additional probe laser. From the time dependence of the SEP signal, the total rates of $O_2^\ddagger$ disappearance were determined for levels up to $v = 26$. For $v = 27$, however, the rate of relaxation was too fast to be directly observed. At this point, they resolved to monitor the population of the lower vibrational states and by assuming a given kinetic model they gave an estimation for the depletion rates of $v = 27$, 28. As a major result within this kinetic model, Wodtke and co-workers [10,11] found a sharp increase in the rates of disappearance of $O_2(v)$ for $v \geq v_c$, where $v_c = 25{-}26$ at $T = 295$ K, and $v_c = 26{-}27$ at $T = 465$ K. Considering that the mentioned vibrational levels were close to the reaction barrier, together with some other considerations [11], they proposed the reaction

$$O_2(X^3\Sigma_g^-, v) + O_2(X^3\Sigma_g^-, v = 0) \rightarrow O_3(X^1A_1) + O(^3P) \quad \text{(R1)}$$

[a] e-mail: jcm@fresno.csic.es

as the responsible mechanism for the sharp increase in depletion rates. This suggestion was supported by theoretical calculations [12,13] for which the vibrational relaxation rates matched the experimental depletion rates for vibrational levels up to $v = 25$. The proposition of reaction (R1) became very attractive to explain the ozone deficit problem [2]. Indeed, atmospheric model simulations [6,14] showed that the ozone deficit could be overcome by this new autocatalitic mechanism. Since then effort was focussed in obtaining reaction rate constants for (R1). It should be mentioned that in the Wodtke's experiments, such a direct measurement could not be performed because ozone was not directly detected.

Recently, we presented a calculation on (R1) in which reaction rate constants at several temperatures were reported [15]. It was found that although reaction occurs it is too slow to account for the sharp increase in depletion rates. Similar conclusions were reached in a preliminary calculation by Balakrishnan *et al.* [16] as well as in more recent works [17,18]. In this paper we present a full description of the reduced dimensionality model used to calculate reaction rate constants and probabilities together with interesting details. The inverse reaction is also investigated within our model in order to compare with available theoretical [16,19–21] and experimental [22] data. In addition, the inelastic process is studied and the results have led us to propose a new explanation [23] of the mentioned experimental jump.

The article is arranged as follows. In Section 2 we describe the two dimensional potential energy surface (PES) on which the quantum reactive and inelastic dynamics is studied, as well as the time-dependent and time-independent methodologies employed. Results indicating the presence of chemical reaction and inelastic probabilities are presented and discussed in Section 3 and our final conclusions are given in Section 4.

2 Theoretical model

2.1 Model Hamiltonian and potential energy surface

In the theoretical treatment of reaction (R1) several considerations must be made. First, it is a very complicated reaction since it involves four heavy atoms that make calculations more difficult and second, it also involves the presence of very excited species. These are reasons that advise the use of reduced dimensionality treatments since even with the present state-of-the-art computer technology it is a very difficult task to perform a full dimensional calculation.

Two degrees of freedom are considered in our reduced dimensionality model: the internuclear distance of the vibrationally excited O_2 molecule, r, and the distance between the centers of mass of the two diatoms, R. The Hamiltonian for these collinear-like Jacobi coordinates is

$$H = -\frac{\hbar^2}{2\mu_R}\frac{\partial^2}{\partial R^2} - \frac{\hbar^2}{2\mu_r}\frac{\partial^2}{\partial r^2} + V(R,r) \qquad (1)$$

where the masses involved are $\mu_r = (m_O m_O)/(m_O + m_O)$ and $\mu_R = (2m_O 2m_O)/(2m_O + 2m_O)$, m_O being the atomic oxygen mass. $V(R,r)$ is an effective PES which we have built from the six-dimensional PES of Varandas and Pais (VP) [24].

The procedure for obtaining $V(R,r)$ consists of minimizing the energy, for fixed values of the two reaction-like coordinates (R,r), and adding the harmonic zero-point energy of the remaining degrees of freedom [25]. We have kept frozen the internuclear distance of the O_2 molecule whose bond is not broken at 2.35 bohr, which represents a compromise between the equilibrium O_2 and O_3 values, so that only the zero-point energies of the bending coordinates are included. Although the method seems straightforward, problems are found to obtain $V(R,r)$ in the products channel region, due to the inadequacy of the coordinates (R,r) to describe the stretching motion of the newly formed O−O bond in ozone. In that region, where r becomes large, it is found during the minimization procedure that for a large range of R the angular coordinates can be varied in such a way that a minimum is found for a geometry close to the O_3 equilibrium. The result is an unphysical product channel well, where the frequency corresponding to the stretching mode of the newly formed bond is too small. It is interesting to notice that two prototypical systems of quantum reactive scattering [26] $H_2 + CN$ and $H_2 + OH$, are characterized by saddle-points where the bond being broken and the bond being formed are nearly collinear and are therefore not strongly affected by the choice of Jacobi coordinates when obtaining the reduced dimensionality potential. Unfortunately the O_2+O_2 system has a non-planar saddle-point which does not resemble aforementioned collinear geometry. To solve the problem we rather perform the minimization procedure using valence coordinates, for which the bond distances and angles are decoupled, and then we transform back to Jacobi coordinates. Following this method we have obtained a smooth PES which properly describes the bond breaking and bond forming process and avoids local (most likely spurious) minima encountered in previous dynamical studies using the VP PES [24,27].

A contour plot of the 2D PES so obtained is shown in Figure 1. The geometry and energy of the saddle point are very close to those of the full dimensional surface. Our zero-point corrected exothermicity and energy barrier values are 4.11 and 4.26 eV, respectively, while those of the VP full dimensional surface are 4.09 and 4.25 eV, respectively.

The aim is to obtain initial state-selected reaction probabilities

$$P_v = \sum_m P_{vm}, \qquad (2)$$

P_{vm} being the state-to-state reaction probability where v indicates the vibrational excitation of the active reactant O_2 and m is related with the vibrational excitation of the bond formed in O_3. In the same way, we are interested in the initial state-selected inelastic probabilities

$$P_v^{ine} = \sum_{v' \neq v} P_{vv'}. \qquad (3)$$

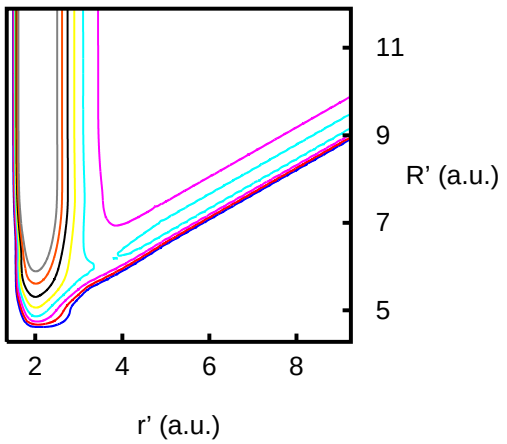

Fig. 1. Contour plot of the reduced dimensionality potential, $V(r', R')$, used in all the calculations presented in this work. r' and R' (in atomic units) are mass-scaled Jacobi coordinates (Eq. (4)). The contours range from 2.25 eV to 5.75 eV with evenly increments of 0.25 eV. The zero of energy corresponds to the minimum of the $O_2 + O_2$ channel.

Next we present two approaches (time-independent and time-dependent) for the dynamical calculations. The rate constants calculation is presented at the end of this section.

2.2 Time-independent calculations

A standard procedure has been used in the time-independent (TI) calculations. The Jacobi coordinates r and R are mass-scaled:

$$r' = (\mu_r/\mu)^{1/2} r, \tag{4a}$$

$$R' = (\mu_R/\mu)^{1/2} R, \tag{4b}$$

(where $\mu = (\mu_r \mu_R)^{1/2}$) and further transformed to hyperspherical (polar) coordinates ρ and δ

$$\rho^2 = r'^2 + R'^2 \tag{5a}$$

$$\tan\delta = \frac{R'}{r'}\cdot \tag{5b}$$

The Schrödinger equation, now depending on ρ and δ, is solved in two steps. First, for a range of ρ values, bound-state problems are solved for the coordinate δ, such that a set of eigenvalues and eigenfunctions depending parametrically on ρ is obtained. The total wavefunction, expanded as a linear combination of the previous eigenfunctions with unknown coefficients depending on ρ, is substituted into the Schrödinger equation leading to a set of close coupled equations which are solved by means of the R–matrix propagation method of Light and co-workers [28]. Applying the appropriate boundary conditions gives the state-to-state reaction probability as the squared modulus of the corresponding S–matrix element.

Although in our model only two degrees of freedom are explicitly treated, the fact that we are dealing with very excited states and that, as it is seen later, reaction and inelastic probabilities are very small for the translational energies of interest, we need to perform a very careful calculation of such small probabilities. In many situations, when hyperspherical coordinates are used approximate boundary conditions (ABC) are applied [29], where boundary conditions are directly imposed in hyperspherical coordinates and the probabilities so obtained are averaged over a range of ρ values. Here, we check this procedure against the use of exact boundary conditions (EBC), where the S–matrix is obtained by projecting the asymptotic scattering wave onto the correct asymptotic vibrational states in Jacobi coordinates [30].

Moreover, we have found that more accuracy and saving in computing time can be gained by the use of "shifted mass-scaled Jacobi coordinates"

$$r'_s = (\mu_r/\mu)^{1/2}(r - r_0), \tag{6a}$$

$$R'_s = (\mu_R/\mu)^{1/2}(R - R_0), \tag{6b}$$

before transforming to hyperspherical coordinates. In this way, (R_0, r_0) are chosen such that a new and more convenient origin of coordinates ($\rho = 0$) is defined. In the present case we have chosen (R_0, r_0) to be the values of the bottom-left corner in Figure 1. This has allowed us to set a smaller grid for the δ coordinate (in comparison with using $(R_0, r_0) = (0, 0)$). In addition, a better rate of convergence to the asymptotic states, as ρ increases, is achieved, since the new δ and ρ coordinates are more decoupled in the asymptotic region than those corresponding to unshifted Jacobi coordinates. To the best of our knowledge, the use of these shifted coordinates has not been reported before.

With regard to the numerical details, the hyperradius is divided into 200 sectors between $\rho = 0.2$ bohr and $\rho = 15.0$ bohr. For each sector the bound hyperspherical "surface states" were obtained using a particle-in-a-box discrete variable representation (DVR) [31] grid of 600 points. The lowest 70 surface states were used in the R–matrix propagation. With these numerical parameters, the reported probabilities and rates are converged within 1% with respect to number of sectors, ρ range, number of DVR points, and number of propagated channels.

2.3 Time-dependent calculations

In the time-dependent (TD) treatment of the reactive process, an initial wave packet describing the state of reactants, $\Psi(R, r, t = 0)$, is propagated in time subject to the time-dependent Schrödinger equation,

$$i\hbar\frac{\partial\Psi}{\partial t} = H\Psi, \tag{7}$$

with the Hamiltonian, H, given by equation (1). The initial wave packet at time $t = 0$ is given by

$$\Psi(r, R, t = 0) = \phi_v(r)\chi(R), \tag{8}$$

where $\phi_v(r)$ is an eigenstate of O_2 and

$$\chi(R) = \left(\frac{2Im\alpha}{\pi\hbar}\right)^{1/4} e^{[-\frac{i}{\hbar}(\alpha(R-R_0)^2+p(R-R_0))]} \quad (9)$$

is a general Gaussian wave packet in Heller's notation [32] that describes the translational degree of freedom, p being the mean momentum along the R coordinate and R_0, the initial position where the Gaussian function is placed, out of the interaction region.

Reaction probabilities can be obtained, as indicated by Zhang *et al.* [33], from the behavior of the time-independent wave function Ψ_E at a dividing surface r_s. This wave function is obtained by Fourier transforming our time-dependent wave packet [32,33]:

$$\psi_E = \frac{1}{a(E)} \int_{-\infty}^{\infty} dt\, e^{iEt/\hbar} \Psi(r, R, t), \quad (10)$$

with

$$a(E) = \iint dr\, dR\, \phi_v^*(r) C e^{-ikR} \Psi(r, R, t=0), \quad (11)$$

where C is an appropriate normalization constant such that $\langle \Psi_E | \Psi'_E \rangle = 2\pi\hbar\delta(E - E')$.

With the above wave function so obtained, the reaction probability is computed as:

$$P_v(E) = \frac{\hbar}{\mu_r} \mathrm{Im} \langle \psi_E | \delta(r - r_s) \frac{\partial}{\partial r} | \psi_E \rangle. \quad (12)$$

In addition, in order to follow the course of the reaction, a time-dependent reaction probability can be extracted from the wave packet calculation

$$P_r(t) = \frac{\hbar}{\mu_r} \mathrm{Im} \langle \Psi(t) | \delta(r - r_s) \frac{\partial}{\partial r} | \Psi(t) \rangle. \quad (13)$$

Concerning the numerical details, a grid of 256 evenly spaced points along the R coordinate and 512 for the r coordinate has been employed. Long propagation times were necessary since wave packets moved along the products valley with very small kinetic energy (note that the energy difference between the saddle point and the bottom of the products valley is rather small). To avoid problems of spurious reflections, we have used an absorbing function [34] of the form $f(R) = \exp(-\beta(R - R_{abs})^2)$, with values $\beta = 10.5$ Å^{-2} and $R_{abs} = 6.35$, for $R \geq R_{abs}$ and $f(R) = 1$ otherwise. Analogously for $f(r)$, a Gaussian function with parameters $\beta = 9.0$ Å^{-2} and $r_{abs} = 5.82$ Å, has been used for $r \geq r_{abs}$, while $f(r) = 1$ has been taken for $r < r_{abs}$. The propagation has been carried out with the "split operator" proposed by Feit and Fleck [35], with typical time steps of 0.01 fs. Concerning the dividing surface given by r_s, we have used r_s values beyond the saddle point (in the direction that goes toward product states), checking that the chosen position does not alter the calculated reaction probabilities.

2.4 Reaction rate constants

We have obtained approximate three-dimensional reaction rate constants using the reduced dimensionality approach of Bowman *et al.* [36]. For the vibrationally state selected collision between $O_2(v)$ with $O_2(v' = 0)$, assuming Boltzmann distributions for the reactant translational and rotational degrees of freedom, the resulting reaction rate constant at temperature T is given by

$$k_v(T) = \frac{f_{elec} Q^{\ddagger}}{h Q_t (Q_{rot})^2} \int_0^{\infty} dE_t\, e^{-E_t/K_B T} P_v(E_t), \quad (14)$$

where the reaction probability (Eq. (2)) is given as a function of E_t, the translational energy. The factor taking into account the electronic degeneracy is taken to be $f_{elec} = 1/3$, since of the nine degenerate states of the reactants (corresponding to the singlet, triplet and quintet states of $(O_2)_2$), only the triplet state correlates with products $O_3 + O$. On the other hand, Q_t is the reactant translational partition function and Q_{rot} is the classical rotational partition function of O_2 [37]. Finally, $Q^{\ddagger} = Q^{\ddagger}_{vib} Q^{\ddagger}_{rot}$ is the vibrational-rotational partition function of the transition state (TS), where

$$Q^{\ddagger}_{vib} = \prod_{s=1}^{3} \left[1 - \exp(-\hbar\omega_s^{\ddagger}/K_B T)\right]^{-1}, \quad (15)$$

and

$$Q^{\ddagger}_{rot} = (\pi I_a I_b I_c)^{1/2} \left(\frac{2K_B T}{\hbar^2}\right)^{3/2}. \quad (16)$$

Since the TS has a nonlinear geometry (it is in fact nonplanar), it is described by an overall rotation together with five vibrational modes. The two vibrational modes correlating with the stretchs of the two O_2 molecules are not included in $Q^{\ddagger}_{vib}$: one of them is explicitly considered in the dynamics; the other one, corresponding to the "spectator" $O_2(v' = 0)$, has been checked to have a negligible effect on the calculated rate constants. Thus, $Q^{\ddagger}_{vib}$ is computed from the three harmonic bending frequencies, (w_s), at the TS. In equation (16), I_a, I_b, I_c are the principal moments of inertia of O_4 at the TS. We have checked that the frequencies and constants of inertia used here are almost identical to those reported by Balakrishnan and Billing [16,21], which is the expected result since they used the same VP PES. In addition, the TS data are fairly similar to those of the *ab-initio* calculation of Lauvergnat and Clary [18].

3 Results and discussion

3.1 The inverse reaction

The inverse of reaction (R1),

$$O(^3P) + O_3(^1A_1) \rightarrow 2O_2(X^3\Sigma_g^-) \quad (R2)$$

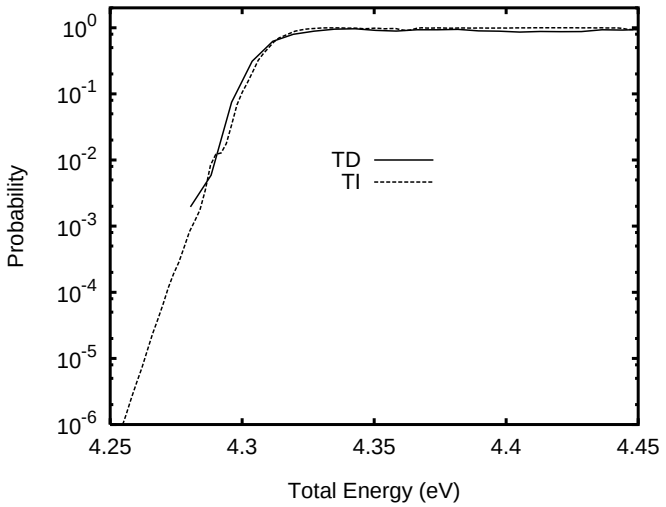

Fig. 2. Time-dependent (TD) and time-independent (TI) initial state selected cumulative reaction probabilities for reaction (R2) (for ozone initially in the ground state) as functions of total energy. Note that the reaction barrier is 4.26 eV. The zero of energy corresponds to the minimum of the $O_2 + O_2$ channel.

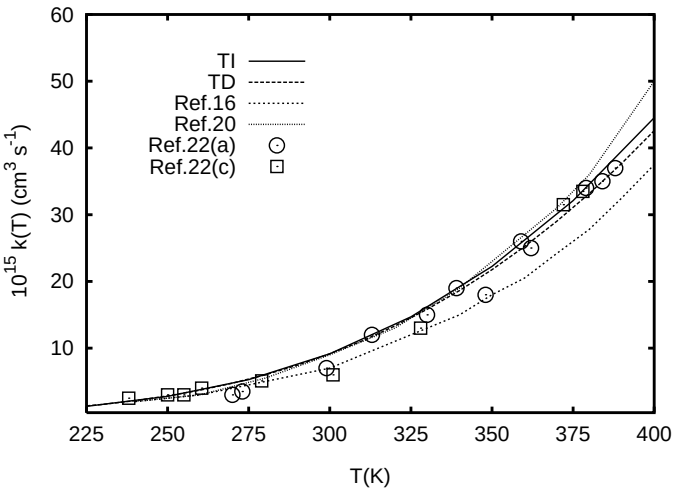

Fig. 3. Thermal rate constants for reaction (R2) (reverse of (R1)), computed with time-dependent and time-independent methods and compared with some theoretical (Refs. [16,20]) and experimental (Ref. [22]) rates.

is a highly exothermic reaction that has been studied by means of different theoretical methods [16,19–21,24] (all of them based on the same VP PES [24]), whose results are in very good agreement with what has been experimentally reported [22]. In order to test our reduced dimensionality model, it is a natural choice to begin presenting the calculations of the rate constants of (R2). Comparison with experiments will also serve as a convenient scenario for the discussion of the reliability of the VP PES.

In Figure 2 we show the cumulative reaction probabilities (starting with the ground state of O_3 and summed to all final product states) computed with time-dependent and time-independent methods. It is seen that both calculations compare quite satisfactorily. It can also be appreciated that, as expected for an exothermic reaction, there is almost no reaction threshold: for a total energy just above 4.26 eV (the saddle point energy, measured from the bottom of the O_2+O_2 valley), the reaction probability rapidly rises reaching almost 1. As a consequence, rate constants are expected to be quite large. Proceeding similarly to the direct reaction, the thermal rate constant (summed over all initial states) for (R2) can be written as

$$k(T) = \sigma_s \frac{f_{elec} e^{\Delta/K_B T} Q^{\ddagger}}{h Q_t Q_{rot} Q_{vib}} \int_0^{\infty} dE\, e^{-E/K_B T} P_{cum}(E) \tag{17}$$

where $P_{cum}(E)$ is the total cumulative reaction probability (sum over all initial and final states) E is the total energy (the zero of energy corresponding in this case to the ground state of O_3), $Q^{\ddagger}$ is the transition state partition function (the same as used for the direct reaction), and Q_t, Q_{rot} and Q_{vib} are the translational, rotational and vibrational, respectively, partition functions of reactants (Q_{vib} is computed accordingly with the above mentioned choice of zero of energy). The geometry and vibrational frequencies of O_3, needed to calculate Q_{rot} and Q_{vib}, where obtained from the full dimensional VP PES and are very close to the spectroscopic values [38]. On the other hand, Δ corrects the barrier height for having kept frozen the internuclear distance of the spectator bond as well as not having included the zero point energy of the corresponding mode, as described in detail in reference [39] for the case of $OH + H_2$. In equation (17), σ_s is the statistical factor, which is assumed to be 2 as in reference [16], and $f_{elec}(T)$ is a factor accounting for the electronic degeneracies of (R2). Its value has been taken as that suggested by Varandas and Pais [24]

$$f_{elec}(T) = \frac{3}{5 + 3\ \exp(-228/T) + \exp(-326/T)}. \tag{18}$$

In Figure 3, we present our calculated rate constants (both from TI and TD calculations) for different temperatures, compared with some theoretical [16,20] calculations as well as experimental measurements [22]. We would like to emphasize two points. First, our rate constants compare well with the variational transition state ones of reference [16], and also with calculations of reference [20], which is a quantum mechanical calculation that involves several approximations as the coupled state and quasi-breathing-sphere. Note that both previous theoretical works also used the VP PES. This result gives us some confidence in the reduced dimensionality treatment employed in this work.

Second, it is seen that theoretical calculations using VP PES show quite a good agreement with experimentally measured rate constants, which indicates that the VP PES is quite reliable. Further confidence on the VP PES comes from the fact, commented before, that recent accurate *ab-initio* calculations [18] predict a geometry for the transition state very similar to that of the VP PES. On the other hand, the major drawback of the VP PES has been addressed in the combined theoretical and experimental study by Mack *et al.* [27], where the main

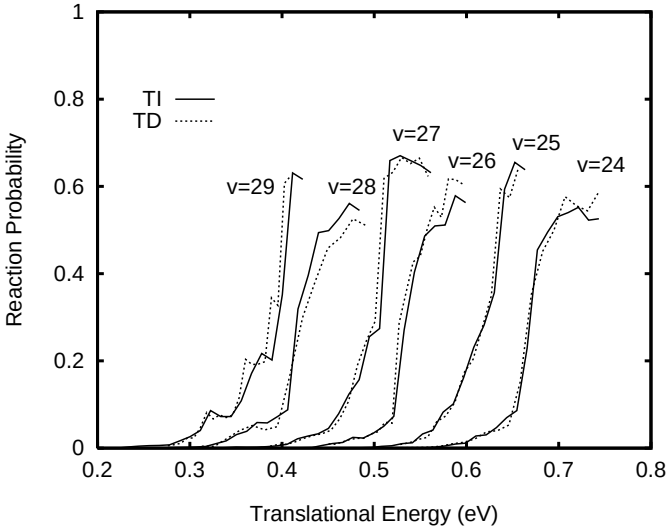

Fig. 4. Time-dependent (TD) and time-independent (TI, EBC) cumulative reaction probabilities for reaction (R1), selected for initial state $O_2(v)+ O_2(v' = 0)$, as functions of translational energy.

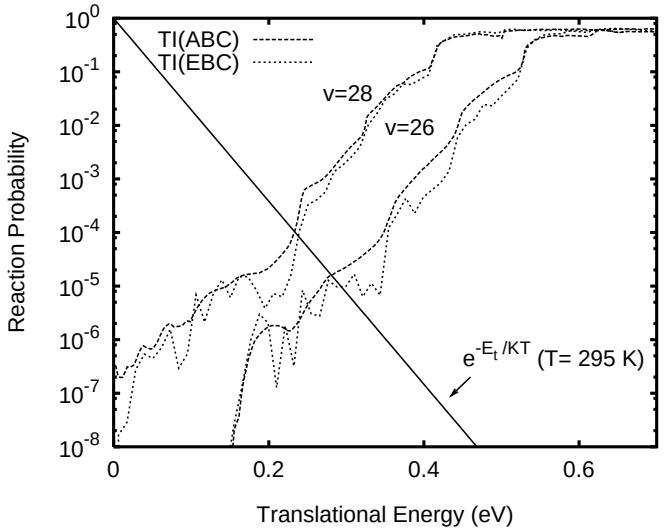

Fig. 5. Time-independent cumulative reaction probabilities (in logarithmic scale) using approximate (ABC) and exact (EBC) boundary conditions as functions of translational energy, for initial states $v = 26$ and 28. In the same figure, the exponential term involved in the calculation of rate constants is also shown for a temperature of 295 K.

conclusion is that the VP PES does not seem to correctly describe the product distribution of (R2), mainly because of the role of the O−O bond which is unbroken during reaction. While in the VP PES such a bond is a mere "spectator", experiments indicate that two vibrationally excited diatomic molecules are produced in reaction, in contrast with a spectator bond model. We see that the VP PES is quite reasonable in describing the TS region and $O_3 + O$ channel, but a deeper attention to the region of $O_2 + O_2$ valley leading to the TS would probably be very valuable.

3.2 The direct reaction

We have studied the reaction (R1) for a large sample of translational energies. In Figure 4, we have plotted the cumulative reaction probabilities summed over final states (Eq. (2)), for different values of the initial vibrational excitation. As can be seen, a remarkable agreement was reached between both TD and TI results (this last one computed using exact boundary conditions). It is evident from that figure that reaction probabilities become quite large once the reaction threshold is reached, but it is seen that such a threshold is found for rather large translational energies and, besides, it depends on the initial vibrational excitation. At this point, it should be recalled that the $v = 28$ state is the first state over the reaction barrier (the vibrational energy of $v = 28$ is 4.33 eV whereas the reaction barrier is at 4.26 eV). Therefore it would be possible, on energy grounds, that reaction occurred at virtually zero translational energy for $v \geq 28$. On the contrary, it is found that a non negligible amount of translational energy is needed to promote reaction, although such a "dynamical" threshold moves to lower translational energies as v increases. In summary, we found that although vibrational energy is very important in order to overcome the barrier (as expected for an endothermic reaction with a late barrier), relative translational energy also plays a role. This is the expected result for a reaction where the combination of masses produces a relatively small skewing angle (see Fig. 1) which reduces the effectiveness of vibrational energy.

In order to calculate reaction rate constants at the temperatures of interest, it is only of relevance the behavior of the reaction probabilities at low kinetic energies. In Figure 5, $v = 26$ and $v = 28$ reaction probabilities are plotted in logarithmic scale, for the two versions of TI calculations (approximate and exact boundary conditions, ABC and EBC, respectively). The exponential term (given in this scale by a straight line) involved in the calculation of the rate constants (Eq. (14)) is also shown in the same figure for a temperature of 295 K. At this temperature, for instance, the range of translational energies below 0.2 eV is the one that contributes more to the integral of equation (14) for the $v = 28$ rate. It is clear that small absolute errors in the probabilities would produce large errors in the computation of rate constants. Hence for this kind of reactions, where probabilities are very small, much care should be exerted in the convergence of rate constants. On the other hand, it can be seen from Figure 5 that the use of (simpler) TI ABC yields significantly good results in comparison with TI EBC, the most important difference being that, given that the ABC involve some averaging, they give smoother probabilities than the use of EBC.

In computational terms, it should be noted that the ABC approach, being simpler, can become time consuming because propagation up to very large ρ values is needed in order to obtain converged results. The EBC method, on the other hand, involves performing energy-dependent

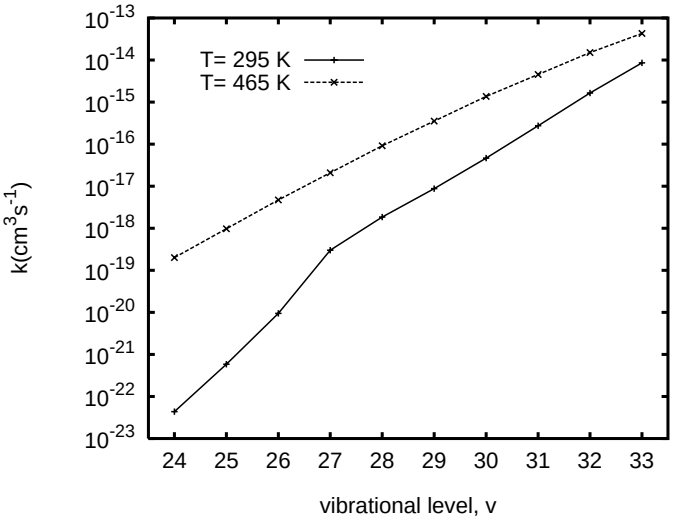

Fig. 6. State selected rate constants for reaction (R1), as functions of the initial vibrational state, v, and for two different temperatures (295 and 465 K). Their values are to small to explain the large values of the experimental depletion rates [11].

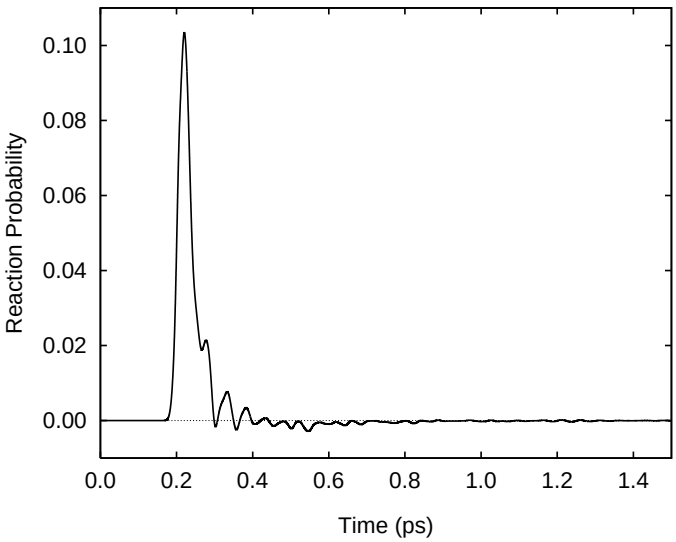

Fig. 7. Reactive flux as a function of time (Eq. (13)), for the time dependent propagation of initial state $v = 28$. Notice that there are times where the backward flux dominates (*i.e.*, negative flux), indicating a recrossing of the wave packet back to the reactants valley.

integrals so it can be less efficient if probabilities are needed over a grid of many energies. Therefore there is a matter of balance between both effects and thus which method presents a better performance depends on the details of the dynamical system. In the present case, where probabilities were computed for a quite large range of total energies, the use of ABC TI method turned out to be less expensive. Regarding the TD calculation, we have checked that it can give as accurate probabilities as the TI method, but at a very high computational cost, since low kinetic energies involve very long propagation times (and much care has to be taken with the accumulation of errors). Moreover, one of the advantages invoked for TD methods that is the choice of the initial state, becomes here a drawback since we are interested in a rather large range of initial vibrational states. If we were interested in just one initial state, the TD method would perform nearly better that the TI one. However, as in the TI scheme virtually all initial vibrational states can be computed at once, the result is an overperformance of the TI method when one is interested in studying several initial states. Although our codes were not completely optimized and we did not attempt to improve their performance, we found that overall the TI method is about 7–10 times more efficient.

In Figure 6, we plot the calculated rate constants (from the TI EBC results), as functions of the initial vibrational excitation and for two different temperatures. As can be seen, the rate constants increase very rapidly with the vibrational excitation indicating that reaction is getting more and more important. Except for the largest temperature and vibrational excitation, their values are, however, too small. In particular, the rate constants for $v = 27$, 28 are far too small compared with those predicted from Wodtke's experimental depletion rates, not even a qualitative jump in the reaction rates for $v > 25-26$ is found as suggested from their experiments. In other words, as recently reported [15], the proposition that reaction (R1) would be the responsible of the observed jump is not supported by our calculations. Same conclusion was reached by Balakrishnan and Billing [16] who employed a semiclassical wavepacket method and, more recently, by Varandas and Wang [17] who carried out full dimensional quasiclassical trajectories, in both cases using the same PES. Moreover, the same negative result was found by Lauvergnat and Clary [18], who obtained reaction rate constants from a new *ab-initio* PES.

At this point, it results interesting to present Figure 7, where the time dependent reaction probability (Eq. (12)) is depicted for a propagation of the $v = 28$ initial state with a central total energy of 4.83 eV. It is seen that, after the main portion of the wave packet crosses the TS, there are times where the backward flux dominates (*i.e.*, is negative), indicating that some portion of the wave packet goes back to the entrance channel. Although a quantitative measurement of the recrossing has not been attempted, we do have checked that the backward flux is larger for lower translational energies. This result suggests that the behavior of the inelastic probabilities can be affected by the TS region (and beyond it in going to the product channel) in the PES, even in the absence of reaction. It can be expected that a more effective energy transfer is produced if the diatomic partners reach the TS region before being inelastically scattered.

3.3 The inelastic process

The conclusion that, although (R1) occurs, it is too slow to explain the experimental jump in depletion rates, together with the suggestion from the TD calculations that the TS may play a role in the inelastic process, have prompted us

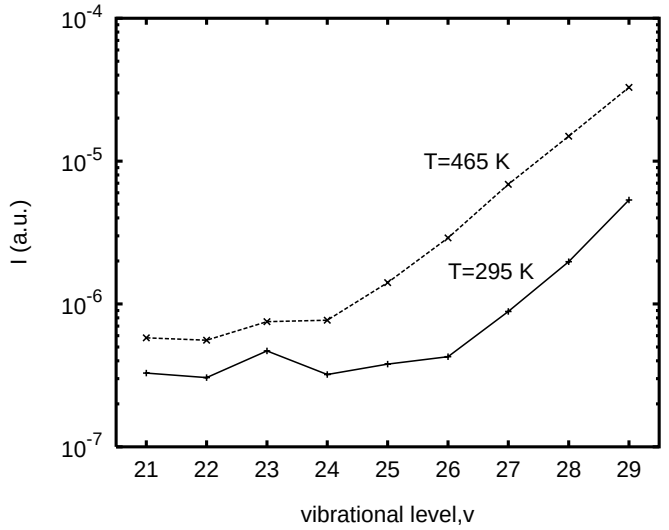

Fig. 8. Integrals defined in equation (19) as functions of the initial state v and for temperatures 295 and 465 K. As such integrals are related with the vibrational relaxation rates, it is suggested that the experimentally observed [11] jump in $O_2^{\ddagger}$ depletion rates could be explained by vibrational relaxation rather than reaction.

to study the inelastic process on the same reduced dimensionality PES.

Inelastic probabilities (summed over all inelastic channels, Eq. (3)) were computed within the TI framework and using exact boundary conditions. In this case we have found, contrarily to what happened in the reactive case, that the use of approximate boundary conditions yields very inaccurate results. This can be understood from the fact that, in the absence of reaction, the inelastic probability is $\approx 1 - P_{elastic}$, so we are actually dealing with the calculation of a state-to-state probability ($P_{elastic}$ in this case), which is usually much more difficult to converge using approximate boundary conditions than a probability involving sums over several states. In order to obtain relaxation rate constants, there are some approaches in the theory of inelastic collisions which are quite similar in spirit to the transition state theory for the reaction dynamics [40]. An "inelastic version" of the reduced dimensionality theory of Bowman [36] can be developed and we are working in that direction. However, insight on the variation of the relaxation rate constants with the initial vibrational excitation at a given temperature can be gained by computing the integral

$$I_{v,T} = \int_0^\infty dE_t \, e^{-E_t/K_B T} P_v^{ine}(E_t). \qquad (19)$$

In Figure 8, the calculated integrals are presented for $T = 295$ and $T = 465$ K. It is noticeable that, contrarily to the reaction rates shown in Figure 6, the results presented in Figure 8 indicate that the vibrational relaxation rates would undergo a jump above $v_c = 26$ and $v_c = 24$ for $T = 295$ and $T = 465$ K, respectively. The present results are in good qualitative agreement with experiment: depletion rates increase quite strongly above a certain vibrational level v_c, which depends on temperature (the experimental values of v_c are $v_c = 24{-}25$ ($T = 295$ K) and $v_c = 26$ ($T = 465$ K). At this point, it is interesting to comment on previous theoretical calculations on relaxation rates. Hernández *et al.* [13] computed explicit values for vibrational-to-translational (V-T) and vibrational-to-vibrational (V-V) rates using an accurate *ab-initio* PES that did not include the reactive channel. They obtained quite a satisfactory agreement with the experimental depletion rates for vibrational excitations below the critical value v_c. For $v > v_c$ their relaxation rates showed a smooth behavior without indication of any jump. The most obvious reason for the jump found in our calculations is that the vibrational relaxation rates undergo an enhancement induced by the reactive channel [41,42].

In order to check the previous statement, we have performed additional test calculations in which the region of the saddle point has not been included (by artificially setting a infinite wall in the PES for those points (r, R) such that $r \geq r_{sp}$, where r_{sp} is the saddle point position). In Figure 9, true (solid lines) and "artificial" (dashed lines) inelastic probabilities are compared for different initial vibrational excitations. It has to be recalled that for the translational energies involved in the calculations (shown in Fig. 9), reaction probabilities are negligible in comparison with inelastic probabilities. First, it can be seen in that figure that the true inelastic probabilities exhibit clear thresholds which shift towards lower translational energies as v increases (as if they were reaction probabilities). The sharp rise in the relaxation rates for $v > v_c$ is now easily explained: v_c is the first vibrational level for which the inelastic threshold falls within the translational energy range relevant at a given temperature. Second, when artificial inelastic probabilities are analyzed, it is found that, up to $v = 24$, the exclusion of the TS region hardly affects the behavior of the inelastic probabilities, whereas for larger v's the artificial probabilities become smaller than the true ones. Therefore, the exclusion of the TS shifts the inelastic threshold towards higher energies and, as a consequence, the jump in relaxation rates is not longer found. In conclusion, although the reactive process is of little importance, the presence of the saddle point region is the key for the enhancement of the relaxation rates.

4 Conclusions

We have carried out quantum mechanical time-dependent and time-independent calculations using a reduced dimensionality model for the reactive and inelastic process given by (R1). The reverse process given by (R2) has also been investigated showing that our model can yield accurate values for the magnitudes of interest, compared with available theoretical and experimental results.

The reaction probabilities and rate constants indicate that at the temperatures of interest there is no noticeable reaction that could explain the experimental findings of a sharp jump in depletion rates of vibrationally excited O_2 in collision with ground state oxygen molecules. The inelastic rates, on the other hand, do show a jump from

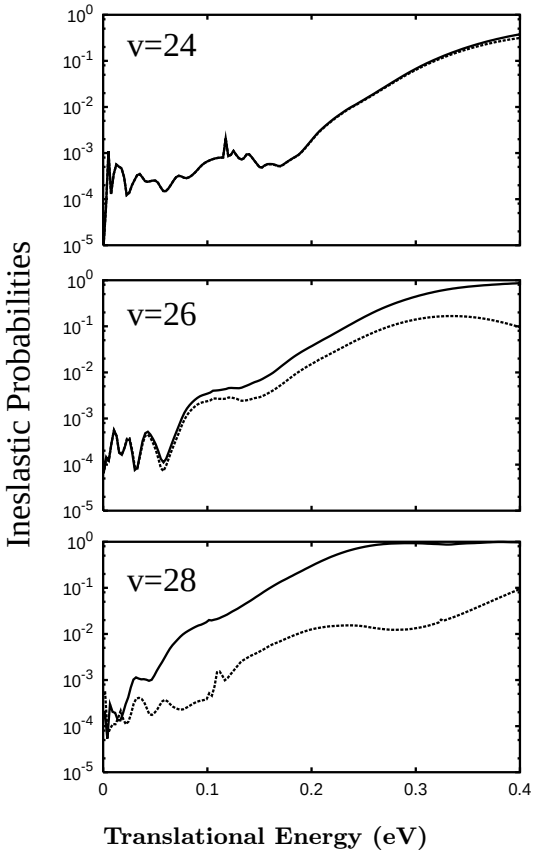

Fig. 9. Cumulative inelastic probabilities for initial states $v = 24$, 26, 28 as functions of translational energy (full lines), compared with analogous probabilities (dashed lines) from calculations where the reaction saddle point region has been artificially excluded. The comparison indicates that the vibrational enhancement in the relaxation rates is induced by the reactive channel.

some vibrational state, v_c, on. For this jump to appear it is crucial to include in the calculations the transition state region of the PES. Thus, although chemical reaction is not very important numerically, the modeling of the inelastic process associated with (R1) needs the inclusion of the reactive channel. Nevertheless, there is still ample room for improvements in both theoretical and experimental sides. In particular, it would be worth a detailed analysis of the PES near the TS towards the $O_2 + O_2$ channel, as well as more experimental data concerning the direct ozone detection or specific state-to-state inelastic transitions in the high vibrational excitation regime.

In the course of this work some other important methodological points have been stressed. First, for reactions with small values of reaction probabilities the errors committed in the computations of the rate constants can be large if a careful examination of reaction probabilities is not carried out for low translational energies. Second, a shift in the origin for the PES helps to obtain well converged probabilities when using hyperspherical coordinates. Third, the use of approximate boundary conditions has proved to be very accurate in the computation of reaction probabilities while gives quite incorrect results in computing inelastic ones.

This work has been partially supported by the DGICYT, (Spain) grant number PB95-0071 and CONACYT (Mexico) grant number 3111P-E9607. RH-L and JC-M wish to thank CSIC (Spain) and CONACYT (Mexico) for the financial support (grant E130.2128) that made possible this collaboration. JE, MIH and JC-M had partial support from European Union grant CI1*-CT94-0128. We would like to thank A.J.C. Varandas for sending us his potential subroutine for the O_4 system. Thanks are also due to D.M. Lauvergnat and D.C. Clary for useful discussions and for a preprint of their related work.

References

1. T.G. Slanger, L.E. Jusinski, G. Black, G.E. Gadd, Science **241**, 945 (1988).
2. C.A. Rogaski, J.M. Price, J.A. Mack, A.M. Wodtke, Geophys. Res. Lett. **20**, 2885 (1993).
3. J. Eluszkiewicz, M. Allen, J. Geophys. Res. **98**, 1069 (1993).
4. P.J. Crutzen, J.U. Grooß, C. Brühl, R. Müller, J.M. Russel III, Science **268**, 705 (1995).
5. M.E. Summers, R.R. Conway, D.E. Siskind, M.H. Stevens, D. Offermann, M. Riese, P. Preusse, D.F. Strobel, J.M. Russell III, Science **277**, 1967 (1997).
6. R.L. Miller, A.G. Suits, P.L. Houston, R. Toumi, J.A. Mack, A.M. Wodtke, Science **265**, 1831 (1994).
7. D. Stranges, X.M. Yang, J.D. Chesko, A.G. Suits, J. Chem. Phys. **102**, 6067 (1995).
8. J.A. Sayage, J. Phys. Chem. **99**, 16530 (1995).
9. H. Park, T.G. Slanger, J. Chem. Phys. **100**, 287 (1993).
10. J.M. Price, J.A. Mack, C.A. Rogaski, A.M. Wodtke, Chem. Phys. **175**, 83 (1993).
11. C.A. Rogaski, J.A. Mack, A.M. Wodtke, Faraday Discuss. **100**, 229 (1995).
12. G.D. Billing, R.E. Kolesnick, Chem. Phys. Lett. **200**, 382 (1992).
13. R. Hernández, R. Toumi, D.C. Clary, J. Chem. Phys. **102**, 9544 (1995).
14. R. Toumi, P.L. Houston, A.M. Wodtke, J. Chem. Phys. **104**, 775 (1996).
15. R. Hernández-Lamoneda, M.I. Hernández, E. Carmona-Novillo, J. Campos-Martínez, J. Echave, D.C. Clary, Chem. Phys. Lett. **276**, 152 (1997).
16. N. Balakrishnan, G.D. Billing, Chem. Phys. Lett. **242**, 68 (1995).
17. A.J.C. Varandas, W. Wang, Chem. Phys. **215**, 167 (1997).
18. D.M. Lauvergnat, D.C. Clary, J. Chem. Phys. **108**, 3566 (1998).
19. H.A. Szichman, A.J.C. Varandas, M. Baer, Chem. Phys. Lett. **231**, 253 (1994).
20. H.A. Szichman, A.J.C. Varandas, M. Baer, J. Chem. Phys. **102**, 3474 (1995).
21. N. Balakrishnan, G.D. Billing, J. Chem. Phys. **104**, 9482 (1996).

22. (a) J.L. McCrumb, F. Kaufman, J. Chem. Phys. **57**, 1270 (1971); (b) D. Davis, W. Wong, J. Lephardt, Chem. Phys. Lett. **56**, 429 (1978); (c) P.H. Wine, J.M. Nicovich, R.J. Thompson, A.R. Ravishankara, J. Phys. Chem. **87**, 3894 (1983).
23. J. Campos-Martínez, E. Carmona-Novillo, J. Echave, M.I. Hernández, R. Hernández-Lamoneda, J. Palma, Chem. Phys. Lett. **289**, 150 (1998).
24. A.J.C. Varandas, A.A.C.C. Pais, in *Theoretical and Computational Models for Organic Chemistry*, edited by S.J. Formosinho, I.G. Czismadia, L.C. Arnaut, Nato ASI Series C (Kluwer, Dordrecht, 1991), Vol. 339.
25. T. Carrington Jr., W.H. Miller, J. Chem. Phys. **81**, 3942 (1984).
26. A.N. Brooks, D.C. Clary, J. Chem. Phys., **92**, 4178 (1990); D. Wang, J.M. Bowman, J. Chem. Phys., **98**, 6235 (1993).
27. J.A. Mack, Y. Huang, A.M. Wodtke, G.C. Schatz, J. Chem. Phys. **105**, 7495 (1996).
28. E.B. Stechel, R.B. Walker, J.C. Light., J. Chem. Phys. **69**, 3518 (1978).
29. J. Römelt, Chem. Phys. Lett. **74**, 263 (1980); *ibid.* **150**, 92 (1988).
30. R.B. Walker, E.F. Hayes, in *The Theory of Chemical Reaction Dynamics*, edited by D.C. Clary (D. Reidel Pub. Co., 1986).
31. J.T. Muckermann, Chem. Phys. Lett. **173**, 200 (1990).
32. E.J. Heller, J. Chem. Phys. **62**, 1544 (1975).
33. D. Zhang, J.Z.H. Zhang, J. Chem. Phys. **101**, 1146 (1994).
34. R. Heather, H. Metiu, J. Chem. Phys. **86**, 5009 (1987); P. Pernot, W.A. Lester Jr., Intern. J. Quantum Chem. **40**, 577 (1991).
35. M.D. Feit, J.A. Fleck Jr., A. Steiger, J. Comput. Phys. **47**, 412 (1982).
36. J.M. Bowman, J. Phys. Chem. **95**, 4960 (1991); J.M. Bowman, Adv. Chem. Phys. **61**, 115 (1985).
37. Laidler, *Theories of Chemical Reaction Rates* (Mc Graw-Hill, 1969).
38. G. Herzberg, *Molecular Spectra and Molecular Structure III: Electronic Spectra of Polyatomic Molecules* (Van Nostran Reinhold Co., New York, 1966).
39. D.C. Clary, J. Chem. Phys. **95**, 7298 (1991).
40. E.E. Nikitin, in *Theory of Elementary Atomic and Molecular Processes in Gases* (Clarendon Press, Oxford, 1974).
41. X. Yang, E.H. Kim, A.M. Wodtke, J. Chem. Phys. **93**, 4483 (1990); *ibid.* **96**, 5111 (1992).
42. I.W.M. Smith, Acc. Chem. Res. **9**, 161 (1976).